Effects of Transglutaminase Cross-linking Process on Printability of Gelatin Microgel-Gelatin Solution Composite Bioink

Kaidong Song[1], Bing Ren[1], Yingnan Zhai[1], Wenxuan Chai[1], Yong Huang[1,2,*]

[1] Department of Mechanical and Aerospace Engineering, University of Florida, Gainesville, Florida 32611, USA

[2] Department of Biomedical Engineering, University of Florida, Gainesville, Florida 32611, USA

[*] Corresponding author: Department of Mechanical and Aerospace Engineering, University of Florida, Gainesville, FL 32611, USA, Phone: 001-352-392-5520, Fax: 001- 352-392-7303, Email: yongh@ufl.edu

Abstract

Three-dimensional (3D) bioprinting has emerged as a powerful engineering approach for various tissue engineering applications, particularly for the development of 3D cellular structures with unique mechanical and/or biological properties. For the jammed gelatin microgel-gelatin solution composite bioink, comprising a discrete phase of microgels (enzymatically gelled gelatin microgels) and a cross-linkable continuous gelatin precursor solution-based phase containing transglutaminase (TG), its rheology properties and printability change gradually due to the TG enzyme-induced cross-linking process. The objective of this study is to establish a direct mapping between the printability of the gelatin microgel-gelatin solution based cross-linkable composite bioink and the TG concentration and cross-linking time, respectively. Due to the inclusion of TG in the composite bioink, the bioink starts cross-linking once prepared and is usually prepared right before a printing process. Herein, the bioink printability is evaluated based on the three metrics:

injectability, feature formability, and process-induced cell injury. In this study, the rheology properties such as the storage modulus and viscosity have been first systematically investigated and predicted at different TG concentrations and times during the cross-linking process using the first-order cross-linking kinetics model. The storage modulus and viscosity have been satisfactorily modeled as exponential functions of the TG concentration and time with an experimentally calibrated cross-linking kinetic rate constant. Furthermore, the injectability, feature formability, and process-induced cell injury have been successfully correlated to the TG concentration and cross-linking time via the storage modulus, viscosity, and/or process-induced shear stress. By combing the good injectability, good feature formability, and satisfactory cell viability zones, a good printability zone (1.65, 0.61, and 0.31 hours for the composite bioinks with 1.00, 2.00, and 4.00% w/v TG, respectively) has been established during the printing of mouse fibroblast-based 2% gelatin B microgel-3% gelatin B solution composite bioink. This printability zone approach can be extended to the use of other cross-linkable bioinks for bioprinting applications.

Key words: Microgel bioink, gelatin, 3D bioprinting, cross-linking, printability, enzyme

1. Introduction

Recently, three-dimensional (3D) bioprinting has emerged as a powerful engineering approach for various tissue engineering applications, particularly for the development of 3D cellular constructs with unique mechanical and/or biological properties [1-4]. During a typical 3D bioprinting process, acellular or cellular bioinks are precisely deposited from a bioprinter as voxel or filament building blocks, layer upon layer, during freeform manufacturing of various 3D constructs, which can be

represented through computer-aided design (CAD) models of tissues/organs to be replaced. The bioink materials are comprised of various materials, including extracellular matrix materials, living cells, and/or any other additives [5] alone or in combination. From an engineering perspective, good bioink materials are expected to possess a repertoire of characteristics for bioprinting. First, they should possess appropriate physiochemical properties, such as shear thinning, appropriate viscosity, in addition to post-printing structural stability [6,7]. Second, they need to have the ability to provide a biocompatible environment in which cellular activities (i.e., encapsulate, migrate, proliferate, and differentiate) can be well developed and maintained [8]. Hydrogel materials such as gelatin, collagen, hyaluronic acid, alginate, and chitosan are excellent bioink materials with a broad range of applications due to their desirable capabilities in mimicking extracellular matrix (ECM) with specific physical and chemical properties.

Of these hydrogel materials, gelatin, a product of denatured and partially hydrolyzed collagen, is one of the most attractive bioink materials with biological cues containing the cell adhesion motif (arginine-glycine-aspartic acid (RGD) sequences) [9] and widely utilized for tissue engineering applications including bioprinting [10-12]. However, the 3D bioprinting of constructs using gelatin or gelatin-based bioinks presents two key engineering challenges. First, gelatin deposition is typically carried out by heating gelatin to be liquid above its normal physiological temperature, followed by immediate delivery into a cold environment for gelation [13] for its thermoreversible property. Such serve temperature conditions may cause some possible temperature-induced cell damage [14] in addition to the effect of temperature drop on the increased ink viscosity. Second, chemically modified gelatin bioinks (such as gelatin methacrylate, GelMA) may require extra chemical modification of native gelatin to introduce the functional groups for controlled physical

or chemical hydrogel formation, and the required cross-linking stimuli such as ultraviolet irradiation might injure living cells [15-18]. To overcome these challenges and improve the gelatin ink printability without sacrificing its biocompatibility, a jammed gelatin microgel-gelatin solution composite bioink has been successfully proposed for bioprinting applications [19,20]. Such a gelatin composite bioink is a yield-stress fluid, comprising a discrete phase of microgels (enzymatically gelled gelatin microgels) and a cross-linkable continuous gelatin precursor solution-based phase containing transglutaminase (TG). The continuous gelatin solution phase may be cellular or acellular, depending on various applications. The jammed gelatin-based microgels function as the rheology modifier for the gelatin solution to provide yield-stress and shear-thinning characteristics. In a jammed microgel system, the microgels can flow and recover (gel-sol and sol-gel transitions) by responding to applied stress without further solidification to keep printed constructs in place. This attractive yield-stress fluid property of the jammed microgel-based composite bioink can minimize the immediate need for any possible cytotoxic cross-linking process during 3D printing, making it ideal for bioprinting applications, in particular, extrusion bioprinting. To form gelatin-based constructs that are stable under physiological conditions, TG, an enzyme with high activity under physiological conditions and catalyzing the formation of covalent bonds between protein molecules, is selected to enzymatically cross-link the gelatin precursor continuous phase of the composite bioink [13,21]. Indeed, enzymatic cross-linking also provides several advantages, such as mild reaction conditions (e.g., neutral pH, aqueous medium, and physiological temperature) and less likely to have unwanted side reactions and cytotoxicity as for chemically modified gelatins (such as ultraviolet light-induced cell damage) [13,15,17].

The objective of this study is to establish a direct mapping between the printability of a jammed gelatin microgel-gelatin precursor solution-based cross-linkable composite bioink and the TG concentration and cross-linking time, respectively, during extrusion bioprinting. For bioprinting studies, rheological properties are usually used as the metrics to evaluate the printability of a bioink due to their critical roles in achieving successful 3D printing processes [22]. Paxton *et al.* [23] described a reproducible method for assessing the printability of bioinks through rheological assessment in terms of the shear-thinning and yield-stress properties. Gao *et al.* [24] investigated the influence of material storage (G') and loss (G'') moduli and their respective ratio ($tan\delta$) on the printability of gelatin-alginate composite ink. Liu *et al.* [25] presented a study to determine the relationship between rheological properties (viscosity, shear moduli, and yield stress) and the 3D printability in a carrageenan-xanthan-starch multi-component printing system. Diamantides *et al*. [26] studied the dependence of storage modulus on the cell density and reported that a higher cell density might result in better printability. More recently, Tan *et al*. [27] evaluated the preheating condition on the printability of gelatin-TG ink in terms of the ink shear moduli and viscosity. However, such identified knowledge of the rheological property-dependent printability cannot be readily applied to the study of the proposed TG-containing cross-linking composite bioink since the TG enzyme-induced cross-linking process gradually affects the ink rheology properties [13,28]. For better use of the proposed cross-linking composite bioink, it is of great interest to develop a direct methodology to evaluate the printability instead of its rheological properties, which is the subject of this study.

Due to the inclusion of TG in the composite bioink, the bioink starts cross-linking once prepared and is usually prepared right before a printing process. As such, the printing time is considered the

cross-linking time. For this work, bioink printability is evaluated based on the following three metrics: injectability, feature formability, and process-induced cell injury. Particularly, the injectability is estimated based on the pressure required for injection, the feature formability is assessed based on the one-dimensional (1D) filament uniformity and 3D structure dimensional fidelity, and the process-induced cell injury during printing is evaluated depending on the post-printing cell viability. Furthermore, a bioink printing zone is identified as a function of the TG concentration and printing time.

2. Materials and Methods

2.1 Ink Preparation

2.1.1 Gelatin microgel preparation

A complex coacervation process was performed to prepare small and uniform gelatin-based microgels. Briefly, a 50% v/v ethanol solution was first prepared using 100% ethanol (Ethanol 200 Proof, Decon Labs, King of Prussia, PA) and deionized water (DI water). Then 2.0% w/v gelatin (100 bloom type B, Fisher Scientific, Hampton, NH), 0.1% w/v gum Arabic (Acacia gum, Sigma-Aldrich, St. Louis, MO), and 0.25% w/v Pluronic F127 (Sigma-Aldrich, St. Louis, MO) were dissolved in the prepared 50% v/v ethanol solution at 50°C and modulated to 7.50 pH by adding 50% v/v sodium hydroxide (NaOH, Sigma-Aldrich, St. Louis, MO). The mixed solution was placed under an overhead stirrer (Fisher Scientific, Hampton, NH) with a speed of 500 rpm to mix overnight while sealed with parafilm to reduce evaporation. TG powders (Moo Gloo TI Transglutaminase Formula, Modernist Pantry, York, ME) were wholly dissolved in deionized (DI) water through a vortex mixer (Mini Vortexer, Fisher Scientific, Hampton, NH), followed by warming in a 37°C bead bath for 30 minutes to yield a 20.0% w/v (TG) stock solution. The

resulting TG solution was added to the gelatin-based microgel slurry at a 1:19 solution/slurry ratio to have a final TG concentration of 1.0% w/v for TG-based enzymatic cross-linking of the gelatin microgels for one day using the overhead stirrer at 500 rpm. The produced slurry was collected into a 50 mL conical tube and centrifuged at 1500 rpm for 5 minutes to compact the cross-linked microgels and remove the supernatant using a centrifuge (5804 R, Eppendorf, Hamburg, Germany). To inactivate TG in the prepared microgels, the 50 mL conical tube containing the gelatin-based microgels was placed in boiling water at 100°C for 20 minutes. The microgels were then resuspended in DI water to wash away Pluronic F127 and ethanol. The microgel slurry was treated three times using a centrifuge at 1500 rpm for 5 minutes to remove excess water. The compacted microgels were dispersed in an equal volume of phosphate-buffered saline (PBS) and autoclaved at 121°C for 60 minutes. The sterilized microgels were centrifuged at 4200 rpm for 10 minutes to remove the supernatant and then stored at 4°C until use.

2.1.2 Gelatin composite bioink preparation

To prepare the gelatin composite bioink, the prepared gelatin microgels were mixed with gelatin powders at 3% w/v as described in a previous study [19]. To investigate the influences of enzyme concentration on the cross-linking speed, different concentrations (5.0, 10.0, 20.0, 40.0, and 80.0% w/v) of the stocked TG solution were added to each composite bioink at a volumetric ratio of 1:19 as described in a previous study [19] to yield different final concentrations of TG (0.25, 0.50, 1.00, 2.00, and 4.00% w/v) right before each use.

2.1.3 Gelatin cellular composite bioink preparation

For determination of the relevance between the maximum extrusion-induced shear stress and cell viability, each cellular bioink was prepared by suspending NIH 3T3 mouse fibroblasts (ATCC, Rockville, MD) in the formulated gelatin composite bioink with a final concentration of 1×10^6 cells/mL for fluorescent staining and 5×10^5 cells/mL for alamarBlue testing. The resuspended 3T3 mouse fibroblast cells were prepared as described in a previous study [19]. Then the different concentrations (20.0, 40.0, and 80.0% w/v) of the stocked TG solutions were added into the composite bioink at a volumetric ratio of 1:19 and mixed thoroughly with a glass rod for final TG concentrations of 1.00, 2.00, and 4.00% w/v for comparison studies.

2.2 Rheology properties

To evaluate the change of rheology properties of the gelatin composite bioinks with different TG concentrations (0.25, 0.50, 1.00, 2.00, and 4.00% w/v) during the cross-linking process, rheological measurements were conducted using a rheometer (Anton Paar MCR 702, Ashland, VA) with a cone-plate measuring geometry. Constant strain sweep tests (1% strain, 1 Hz frequency) were conducted to record the relationship between the storage modulus G' and cross-linking time. To explore the viscosity variation during the cross-linking process, steady shear rate sweeps (from 0.01 to 100 s^{-1}) were conducted every hour to reach a specified low strain (1%). The measuring temperature was set the same as the printing temperature of 25°C for all tests.

2.3 Printing protocols

All printing work was completed through a ball screw-based extrusion printer (Engine SR, Hyrel3D, Norcross, GA). To evaluate the single filament uniformity and dimensional fidelity of 3D tubular structures due to the cross-linking process during printing, the prepared composite

bioinks with different concentrations of the TG stock solution (0.25, 0.50, 1.00, 2.00, and 4.00% w/v TG) were printed through a 19-gauge nozzle (0.686 mm inner diameter, EFD Nordson, Vilters, Switzerland) at a speed of 1 mm/s at room temperature (approximately 25 ℃).

The printing path code for the single 1D filament uniformity evaluation was manually generated in custom G-code scripts. For the designed 3D tubular structure (4.12 mm height, 8.6 mm outer diameter, and 6 mm inner diameter), the structure was first modeled using SolidWorks (Dassault Systemes, Waltham, MA) and then saved as an STL file for uploading into the printer. The experimental model contained in the STL file was sliced by the embedded slicer software of the Hyrel 3D printer (Slic3r tools of the Repetrel control). Once slicing was completed, the G-code was generated automatically by the printer.

2.4 Feature formability analysis

For 1D filament structures, a dimensionless number defined as uniformity ratio (U_r) was used to quantify the morphology of printed 1D filaments by calculating the ratio of the pixel area of a printed filament over the total pixel area of a perfectly deposited filament (that is, a rectangular area). Photographic images of each printed filament were analyzed using ImageJ (NIH, Bethesda, Maryland) to yield the values of pixel area to determine U_r. For the 3D tubular structures, the dimensional fidelity was quantified by comparing the measured height and roundness to the designed values using ImageJ.

2.5 Cell viability

For determination of the relevance between the maximum extrusion-induced shear stress and cell viability, the cellular composite bioinks were extruded into a 96-well plate at the following times: 0.0, 0.5, 1.0, 1.5, and 2.0 hours after the cross-linking process started (that is, after mixing) and incubated for five days in a complete culture medium [Dulbecco's modified Eagle's medium (Sigma-Aldrich, St. Louis, MO) supplemented with 10% w/v fetal bovine serum (HyClone, Logan, UT)] in a humidified 5.0% CO_2 incubator at 37°C. The cell culture medium was changed on the third day.

The cell viability was quantified on Day 5 using the alamarBlue assay (ThermoFisher Scientific, Waltham, MA), and the incubation time was extended to 12 hours as per the manufacturer's protocol. The positive control was prepared by directly culturing the cellular composite bioink in the 96-well plate, and the negative control was prepared by culturing the acellular composite bioink in the 96-well plate. A fluorescence microplate reader (Synergy HT, Biotek, Winooski, VT) was used to measure the fluorescence intensity, and the cell viability was calculated based on the fluorescence intensity relative to the control as

$$Cell\ viability = \frac{Fluorescence\ intensity\ of\ test\ sample - fluorescence\ intensity\ of\ negative\ control}{Fluorescence\ intensity\ of\ positive\ control - fluorescence\ intensity\ of\ negative\ control}.$$

Extruded cells using 1.00% w/v TG were also imaged using fluorescein diacetate (FDA) (Sigma Aldrich, St. Louis, MO) (live, the green color) and Hoechst 33342 (Sigma Aldrich, St. Louis, MO) (nuclei, the blue color) on Day 5. The fluorescent images were captured using a fluorescence microscope (EVOS FL, ThermoFisher Scientific, Waltham, MA). The cell viability was further calculated based on the fluorescent images by dividing the total number of the green-stained cells with the summation of green-stained and blue-stained cells, which was used to compare with the results from the alamarBlue assay.

3. Effects of TG Cross-linking Kinetics on Shear Moduli and Viscosity

3.1 Gelatin cross-linking mechanism

Gelatin precursor can form hydrogel through physical interactions between the inner helical regions of the protein. During cooling, physical cross-linking occurs through the transition from disorder to order, as random coil gelatin molecules seek to return to an ordered triple helix structure [29,30], as shown in **Figure 1a(i)**. This gelatin hydrogel has a thermoreversible physically cross-linked biopolymer network supported primarily by the hydrogen bonding zones. Many factors may affect the gelatin hydrogel strength, such as the concentration and type of gelatin, and the temperature/time history of the sample. For cytocompatibility and bond stability [13,21], TG was used to create a more thermally stable hydrogel through catalyzing the formation of covalent N ε-(ϒ-glutamyl) lysine amide bonds between single strands of gelatin proteins to form a permanent TG-based enzymatically cross-linked network of polypeptides [31] as shown in **Figure 1a(ii) and 1b**. The functional independence of TG to calcium ions or proenzymes and its high level of activity over a wide range of pH values (between 5 and 8, max activity ~90%) and temperatures (0 to 60°C, max activity at 50°C) make TG a good cross-linking material for various cell encapsulation and gel formation applications including the gelatin solution [32-34], making it an ideal cross-linking agent for gelatin composite bioink printing.

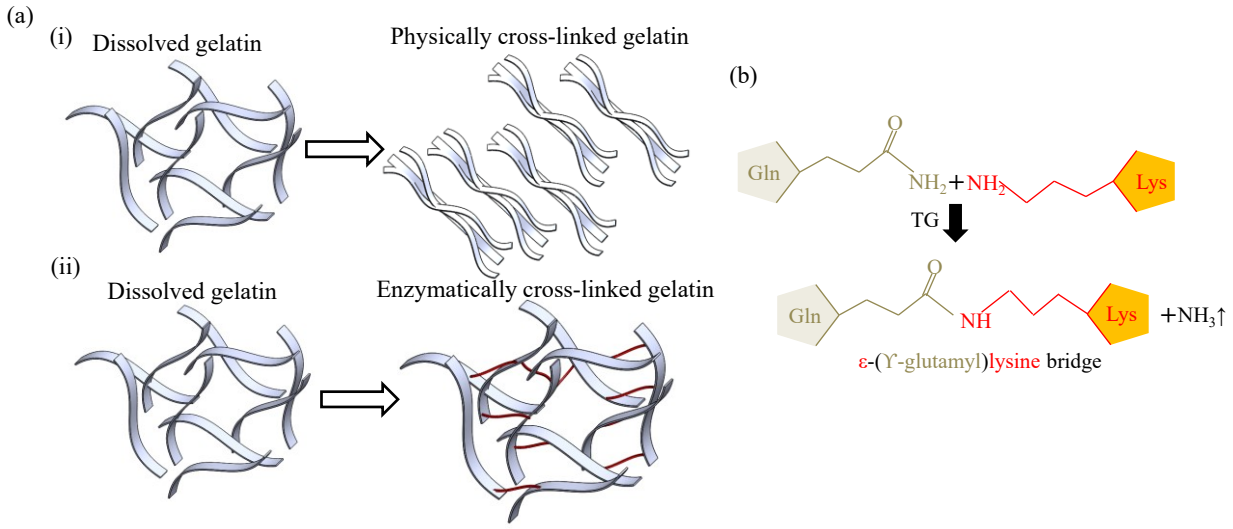

Figure 1. Schematic of gelatin cross-linking processes. (a) (i) physical and (ii) enzymatic cross-linking of gelatin. (b) TG-enabled covalent bond formation among protein molecules.

3.2 Determination of effects of TG cross-linking kinetics on shear moduli and viscosity

To establish a relationship between the enzyme kinetics and printability during the printing of the proposed composite bioink, the effect of enzyme kinetics on rheological properties is first modeled using the Michaelis-Menten kinetics model. This model is utilized to capture the enzyme kinetics involving the binding of enzyme *E* (TG) to substrate *S* (gelatin protein) to develop a TG-based enzymatically cross-linked product *P* (cross-linked gelatin proteins via N ε-(ϒ-glutamyl) lysine amide covalent bonds) [35] as follows:

$$E + S \underset{k_r}{\overset{k_f}{\rightleftarrows}} ES \xrightarrow{k_{cat}} E + P \tag{1}$$

which can be simplified as [36]:

$$E + S \xrightarrow{k} E + P \tag{2}$$

where k_f (forward rate constant), k_r (reverse rate constant), k_{cat} (catalytic rate constant), and k (cross-linking kinetic rate constant) represent the rate constants. It is a reversible process for

enzyme-substrate binding, which is represented with double arrows between *S* (substrate) and *ES* (enzyme-substrate composite). The single forward arrow indicates the *P* (product) formation.

According to the fractal kinetic model [37,38], the cross-linking reaction rate is assumed to be of first order in nature [39]. If the concentrations of substrate and product are represented by $S_c(t)$ and $P_c(t)$, respectively, their first-order rate equations can be formulated as a function of time *t* with:

$$\frac{dS_c(t)}{dt} = -kS_c(t), \text{ and } S_c(0) = S_0 \tag{3}$$

$$\frac{dP_c(t)}{dt} = kS_c(t) \tag{4}$$

with

$$P_c(t) = S_0 - S_c(t) \tag{5}$$

where S_0 is the initial concentration of *S*. By solving Equations (3) and (4) and taking $P_c(0) = 0$, the dynamic product concentration $P_c(t)$ can be determined using:

$$P_c(t) = P_\infty[1 - e^{-kt}] \tag{6}$$

where P_∞ is the equilibrium or final concentration of *P*. Given the storage modulus $G'(t)$ is proportional to $P_c(t)$ [40], the dynamic storge modulus can be represented by:

$$G'(t) - G_0' = (G_\infty' - G_0')[1 - e^{-kt}] \tag{7}$$

where G_0' and G_∞' are the initial and equilibrium values of the storage modulus, respectively.

By substituting the normalized storage modulus Γ' [41] as defined by Equation (8) into Equation (7), an exponential equation of Γ' (Equation (9)) is obtained:

$$\Gamma' = \frac{G'(t) - G_0'}{G_\infty' - G_0'} \tag{8}$$

$$\Gamma' = 1 - e^{-kt} \tag{9}$$

Given that the cross-linking process is known to have first-order kinetics [40,42], the normalized viscosity μ_N [43] as defined by Equation (10) is simplified to follow an exponential equation of the cross-linking time (Equation (11)) as experimentally observed:

$$\mu_N = \frac{\mu - \mu_0}{\mu_\infty - \mu_0} \tag{10}$$

$$\mu_N = 1 - e^{-kt} \tag{11}$$

where μ, μ_0, and μ_∞ are the instant, initial, and equilibrium values, respectively, of the composite bioink viscosity.

Based on the average cross-linking kinetic rate constant k values for each TG concentration as acquired based on Equations (9) and (11), a linear relationship between k and the TG concentration ($Y_{E/C}$) is established using the least squares error (LSE) method [41,44] and represented as:

$$k = aY_{E/C} \tag{12}$$

where a is the constant to be determined. Once a is determined experimentally, the kinetic rate constant k values can be predicted for a given TG concentration by using Equation (12), and the corresponding shear moduli and viscosity can be further predicted as well based on Equations (9) and (11).

3.3 Cross-linking model calibration

Figure 2 depicts the flow chart of the steps to determine the storage modulus and viscosity models of the gelatin composite bioink. For a given concentration TG composite bioink, rheology measurements are first conducted to determine the storage modulus and viscosity values as a function of time during the cross-linking process. By fitting the storage modulus and viscosity values into Equations (9) and (11), respectively, the cross-linking kinetic rate constant k is determined for each composite bioink with a different TG concentration. Then the resulting cross-linking kinetic rate constants are fitted as a linear relationship with the TG concentration ($Y_{E/C}$) based on Equation (12). Finally, the k value is substituted back into Equations (9) and (11) to determine the storage modulus and viscosity models, respectively.

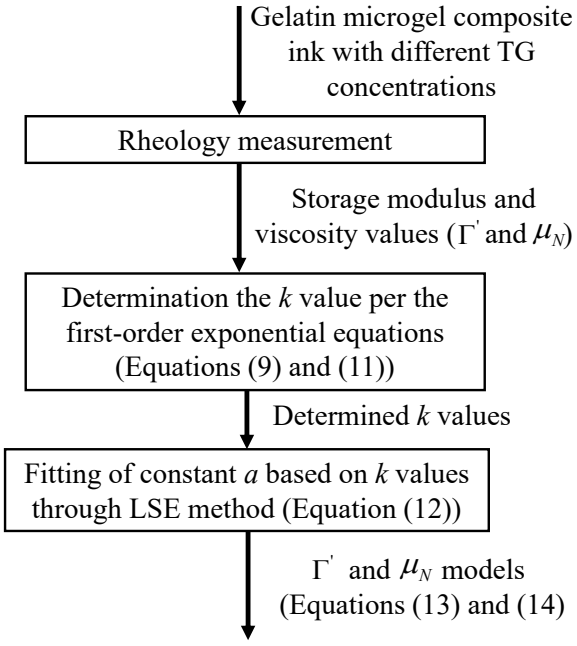

Figure 2. Steps for the determination of shear modulus and viscosity models.

Figure 3a and **3b** shows the normalized storage modulus Γ′ and viscosity μ_N as measured for the gelatin composite bioink with different TG concentrations (0.25, 0.50, 1.00, 2.00, and 4.00% w/v)

at 25°C (room temperature and working temperature) It shows that with TG addition, the storage modulus and viscosity of the composite bioink increase under the enzymatically cross-linking effect, and this increase is dependent on the incubation time and TG enzyme concentration. A plateau value may be reached if enough cross-linking time is given to build up the polypeptide networks for a given TG concentration. **Figure 3c** shows the fitted k values using Equations (9) and (11) as seen from **Figure 3a** and **3b**, which is further listed in **Table 1**. Then the cross-linking kinetic rate constant k is further fitted as a linear function of TG concentrations ($Y_{E/C}$) based on Equation (12), and the determined a value is 0.19. As such, the normalized storage modulus and viscosity models are determined as follows:

$$\Gamma' = 1 - e^{-0.19 Y_{E/C} t} \tag{13}$$

$$\mu_N = 1 - e^{-0.19 Y_{E/C} t} \tag{14}$$

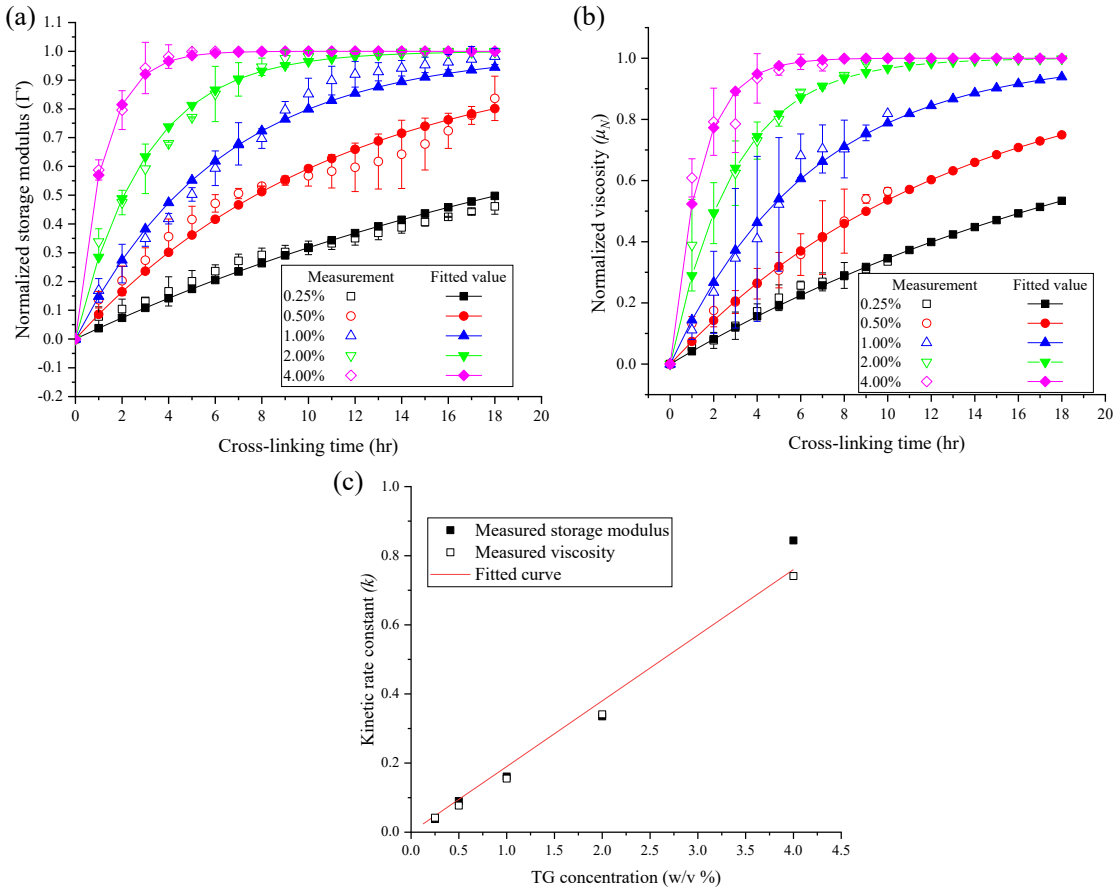

Figure 3. Rheological measurements. (a) Normalized storage modulus Γ′ and (b) normalized viscosity μ_N under different TG concentrations during the cross-linking process. (c) Effect of the TG concentration on the cross-linking kinetic rate constant.

Table 1. Cross-linking kinetic rate constant k.

TG concentration (% w/v)	Kinetic rate constant k determined based on storage modulus (h^{-1})	Kinetic rate constant k determined based on viscosity (h^{-1})
0.25	0.038	0.042
0.50	0.090	0.077
1.00	0.161	0.155
2.00	0.335	0.341
4.00	0.844	0.741

4. Effects of TG-dependent Rheological Properties on Printability

This section evaluates the printability of the designed gelatin composite bioink based on three matrices: injectability, feature formability, and process-induced cell injury during extrusion bioprinting.

4.1 Evaluation of Effects of TG concentration and printing time on injectability

Injectability is one of the important metrics for a successful extrusion bioprinting process and refers to the capability of bioinks to be smoothly injected through a combination of syringe and cannulated needle. For this study, the injectability is evaluated based on the pressure needed for successful injection, which is largely dependent on the bioink viscosity as being related to the resistance of fluid flow to an applied force [45]. The injection pressure can be calculated according to the Hagen-Poiseuille equation [46,47]:

$$P_I = \frac{128\mu LQ}{\pi d^4} \tag{15}$$

where P_I is the pressure, μ is the viscosity, L is the length of needle (25.7 mm), Q is the volume flow rate (0.3694 mm^3/s), and d is the inner diameter of dispensing nozzle (0.686 mm). It is found that a pressure higher than 440 kPa may cause unstable extrusion like an uncontrollable extrusion volume and discontinuous filament, resulting in low-quality printing. As such, a bioink is rated as injectable (high injectability zone) (0-440 kPa) or difficult to inject (low injectability zone) (> 440 kPa) per a similar injectability study [45] and this threshold pressure value may need to be adjusted for different printers.

The proposed composite bioink is non-Newtonian [20]; for the modeling purpose, its viscosity at a given cross-linking time is simply modeled using a power-law model [48,49]:

$$\mu = k_i \dot{\gamma}^{n-1} \tag{16}$$

where k_i is the flow consistency index, and n is the power-law index. By fitting the measurement data into Equation (16), the power-law index n can be simplified as a constant (0.20), and the flow consistency index can be determined as a function of $Y_{E/C}$ and t as follows:

$$k_{iN} = 1 - e^{-0.19 Y_{E/C} t} \tag{17}$$

$$k_{iN} = \frac{k_i - k_{i0}}{k_{i\infty} - k_{i0}} \tag{18}$$

where k_{iN}, k_{i0}, and $k_{i\infty}$ are the normalized, initial (330 Pa·sn), and equilibrium values (1,955 Pa·sn), respectively, of the flow consistency index.

The printing shear rate ($\dot{\gamma}$) of the composite bioink can be estimated as 11.66 s^{-1} according to Equation (19) [50,51]:

$$\dot{\gamma} = \frac{32Q}{\pi d^3} \tag{19}$$

As seen from the rheology measurements (**Figure 3b**), the viscosity of the gelatin composite bioink increases during the cross-linking process, and the viscosity at a given time can be estimated based on Equation (14) and Equation (16) and other rheological properties such as the initial viscosity of μ_0= 47 Pa·s and equilibrium viscosity of μ_∞= 274 Pa·s as obtained from the rheology test under the shear rate of 11.66 s^{-1}. Then the injection pressure is shown in **Figure 4** as a function of cross-linking time for different TG concentrations. As expected, all composite bioinks are injectable (high injectability zone) initially. As the cross-linking process progresses, the composite bioinks gradually become difficult to inject as evaluated based on the required injection pressure. When the printing time increases, the composite bioinks change from injectable to less injectable, especially for higher TG concentration bioinks. Based on the pressure threshold of 440 kPa, a low injectability zone is defined. As seen from Figure 4, the composite bioinks take 14.48, 6.58, and 3.03 hours to reach the low injectability zone for 1.00, 2.00, and 4.00% w/v TG, respectively, while the composite bioinks with low TG concentrations (0.25 and 0.50% w/v) are always highly injectable (high injectability zone) during the evaluation window due to their slow cross-linking process. The injection pressure-based injectability zone can be further determined based on the bioink viscosity as 250 Pa·s using Equation (15), which is equivalently 0.90 for the normalized viscosity. As such, the high injectability zone can be determined by meeting the following criterion:

$$e^{-0.19Y_{E/C}t} \geq 0.10 \tag{20}$$

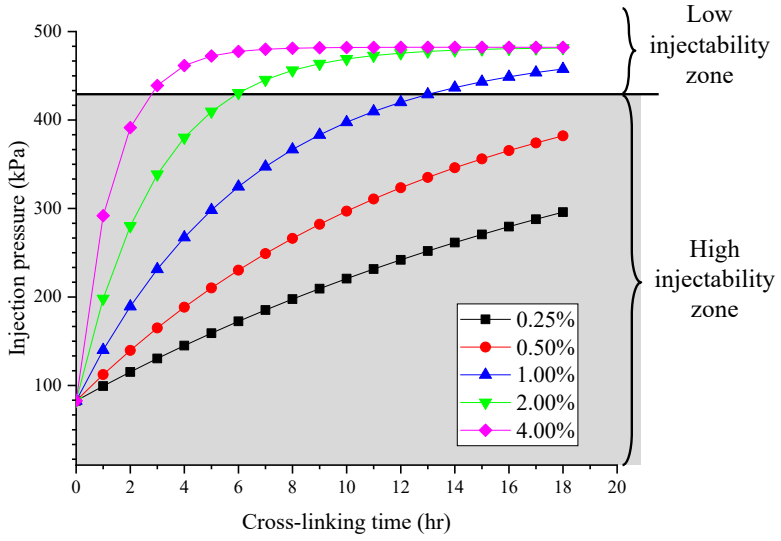

Figure 4. Injectability of the composite bioink as a function of printing time.

4.2 Evaluation of TG concentration and printing time on feature formability

Feature formability is used to describe the ability of a bioink to print in a way that produces the desired print results, including the filament uniformity and structure dimensional fidelity, for a particular application [52]. For the proposed gelatin composite bioink, its feature formability was evaluated in terms of the 1D filament uniformity and the dimensional fidelity of 3D tubular structures as a function of the cross-linking time, which is also the printing time.

4.2.1 1D filament uniformity analysis

As illustrated in **Figure 5a** and shown in **Figure 5b**, there are three types of filament morphology due to the cross-linking process during printing. As the cross-linking time increases, the filament morphology may change from well defined to irregular to broken eventually when printed at

different cross-linking times. For the composite bioinks with high TG concentrations, the experiments were stopped after a broken filament appeared. The area inside the dashed rectangle designates a perfectly extruded uniform filament, which is utilized to calculate the uniformity ratio (U_r) as previously described. **Figure 5c** shows the calculated U_r values of the gelatin composite bioink with different TG concentrations at different cross-linking times. With the decrease of the U_r value, the printed filaments show more and more irregular morphologies. The U_r value above 0.9 is considered acceptable (marked as a shaded region) in this study since such a printed filament shows a well-defined filament morphology. As such, the gelatin composite bioinks cross-linked with 0.25 and 0.50% w/v TG show good feature formability during the 10-hour printing window as investigated, while the other bioinks may not be good for printing after a certain cross-linking time as seen from **Figure 5c**.

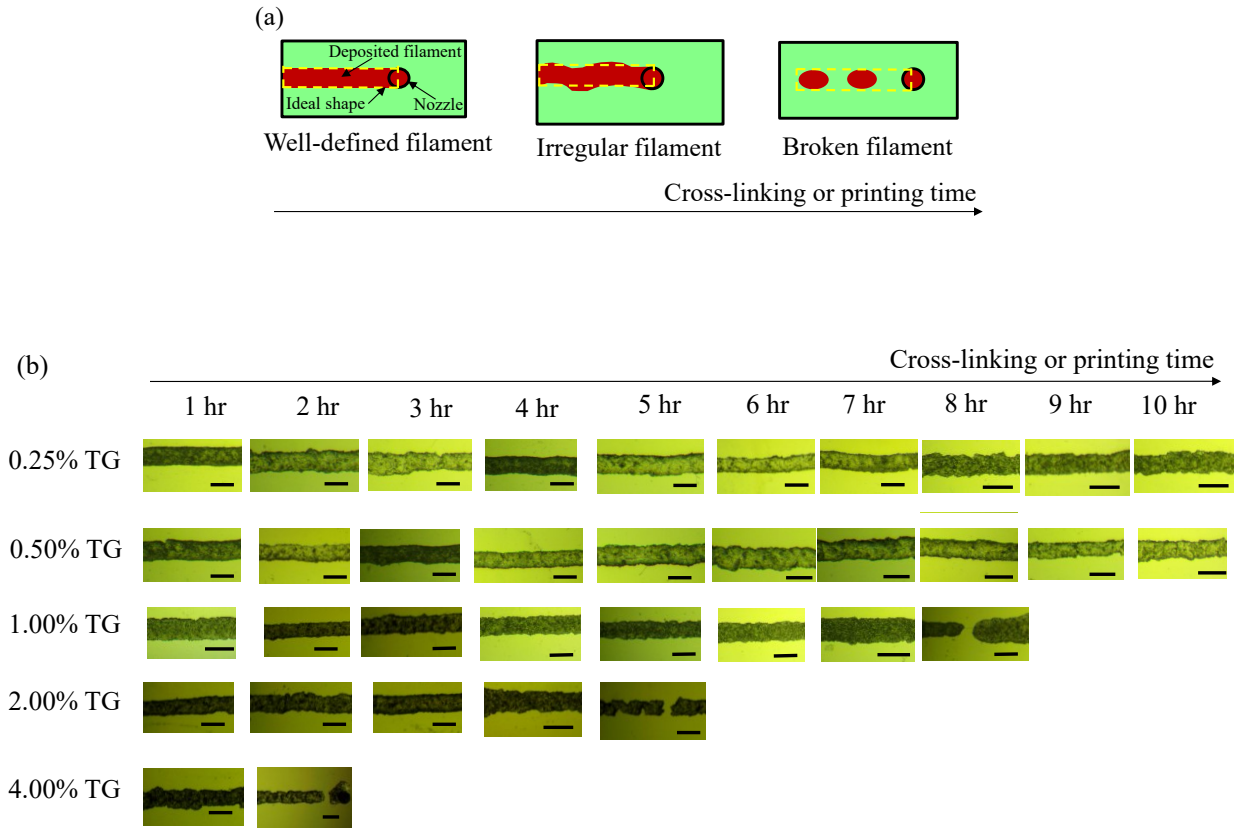

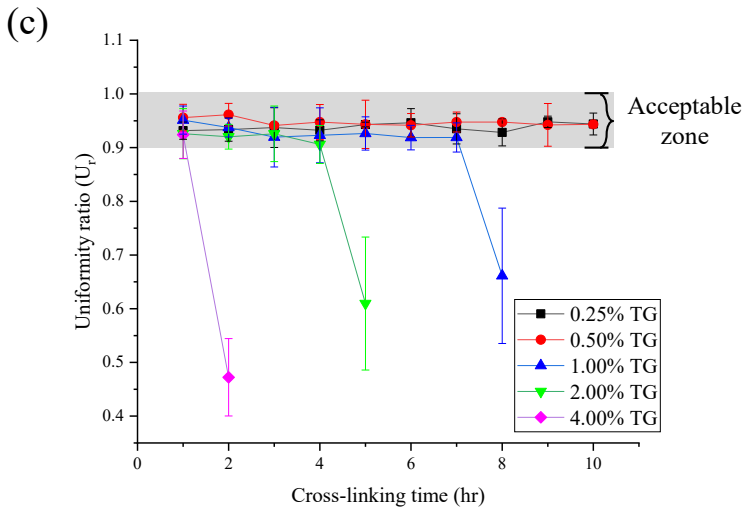

Figure 5. 1D feature formability as a function of cross-linking time. (a) Schematics of 1D filament morphology as a function of the cross-linking time. (b) Different extruded 1D filaments (scale bars: 1 mm). (c) Filament uniformity ratio of the composite bioinks at different cross-linking times.

4.2.2 3D tubular structure dimensional fidelity analysis

Hollow tubular structures were further printed to investigate the effect of the cross-linking process on the feature formability based on the structure dimensional fidelity. **Figure 6a** shows the front and top views of the structures printed using the composite bioinks with different TG concentrations at different cross-linking times. As expected from the 1D filament uniformity study, the dimensional fidelity of the 3D tubes changes from well-defined to irregular to broken at different times depending on the TG concentration. **Figure 6b** and **6c** shows two dimensional fidelity values, that is the normalized tube height (tube height value to designed value) and roundness values, respectively. Similar to the 1D cases, the range of 0.9-1.1 for the normalized tube height and the range of 0.9-1.0 for the normalized roundness are considered acceptable for

the printed tubes. The two acceptable ranges define the corresponding permissible printing times for each composite bioink.

4.2.3 Feature formability analysis

Prior work shows that the storage modulus is highly correlated with the feature formability [49] as the storage modulus corresponds to the mechanical energy stored within a material, which contributes to the stiffness of the material. As such, as the storage modulus increases, the behavior of the composite bioink becomes more and more like a solid, adversely affecting both the filament morphology and dimensional fidelity. As shown in **Figures 5** and **6**, the composite bioink with 1.00, 2.00, and 4.00% w/v TG can be successfully printed for 7, 4, and 1 hours, respectively, and their normalized storage modulus (Γ') values are 0.68, 0.63, and 0.59, respectively as seen from **Figure 3a**. However, these composite bioinks cannot have good filament uniformity or dimensional fidelity after a cross-linking time of 8, 5, and 2 hours, and their corresponding normalized storage modulus (Γ') values are 0.72, 0.73, and 0.80, respectively (**Figure 3a**). Based on the above observations, a normalized storage modulus Γ' value of 0.70 at a given cross-linking time is selected as a threshold to determine whether good feature formability can be achieved. Based on this threshold value and Equation (13), the good feature formability zone can be determined by meeting the following criterion:

$$e^{-0.19Y_{E/C}t} \geq 0.30 \tag{21}$$

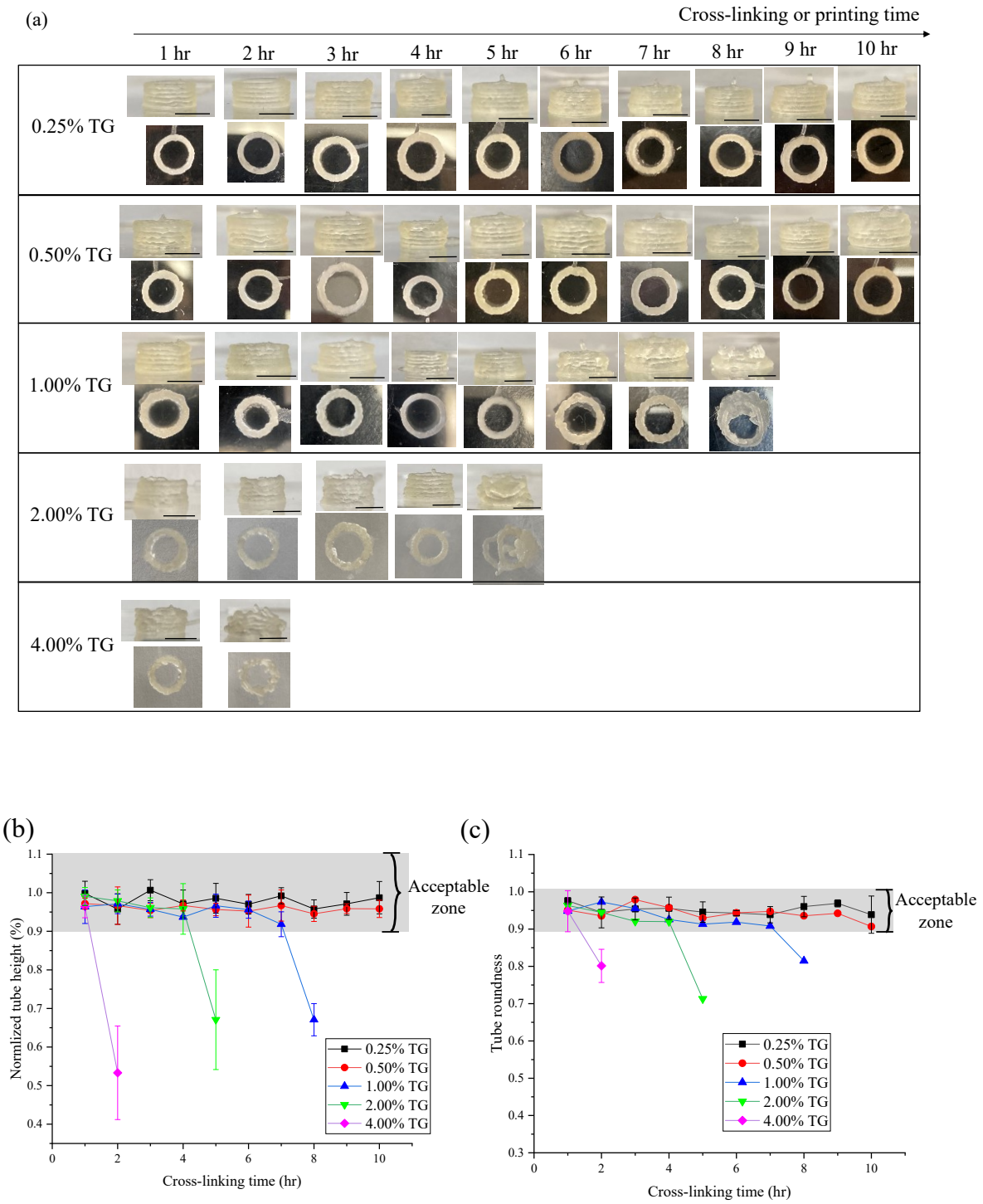

Figure 6. Feature formability over time for 3D tubular structures. (a) The front and top views of printed 3D tubular structures (scale bars: 5 mm). (b) The normalized tube height (tube height value to designed value) and (c) tube roundness.

4.3 Evaluation of TG concentration and printing time on process-induced cell injury

Figure 7a shows the fluorescent images of the cells printed using the 1.00% w/v TG-based cellular composite bioink after different cross-linking times (0, 0.5, 1.0, 1.5, and 2.0 hours) and further incubated for five days. Since its cell viability values determined using fluorescent staining are very close to the results from the alamarBlue test as seen from **Figure 7b**, the cell viability values after five-day incubation are all reported by the alamarBlue test for the sake of simplicity and shown in **Figure 7b**. In general, the cell viability decreases significantly when the cellular composite bioink is printed after different cross-linking times (0, 0.5, 1.0, 1.5, and 2.0 hours), and this dependence is further related to the shear stress needed for extrusion printing using the composite bioink at cross-linking stages. Since the 0.25 and 0.50% w/v TG-based cellular composite bioinks may have a too long cross-linking time and are not practical for bioprinting applications, they were not investigated herein.

Generally, mechanical loading, especially the mechanical shear stress, which causes the material or bioink to deform parallelly to the direction of shear stress, is considered to be a major cause of cell damage/death during bioprinting (including extrusion bioprinting herein) [4,53-58]. The shear stress during the extrusion process changes due to the gradual cross-linking process of the composite bioink in this study. The shear stress (τ) can be computed as the product of viscosity (μ) and shear rate ($\dot{\gamma}$) and simplified as follows based on Equation (16):

$$\tau = k_i \dot{\gamma}^n \tag{22}$$

By assuming a laminar flow during extrusion bioprinting, the velocity profile of the non-Newtonian shear-thinning composite bioink can be estimated quantitatively by the following equation [59]:

$$v = \frac{Q}{\pi R^2}\frac{3n+1}{n}\left(1-\left(\frac{r}{R}\right)^{\frac{n+1}{n}}\right) \tag{23}$$

where $R = \frac{d}{2}$ is the nozzle radius, and the coordinate r is the radial position and $r = 0$ denoting the center of the dispensing nozzle. The shear rate $\dot{\gamma}(r)$ can be determined by the gradient of the velocity as:

$$\frac{dv}{dr} = \dot{\gamma}(r) = \frac{Q}{\pi R^2}\left(3+\frac{1}{n}\right)\frac{r^{\frac{1}{n}}}{R^{\frac{n+1}{n}}} \tag{24}$$

When $r = R$, the maximum shear rate $\dot{\gamma}_{max} = \dot{\gamma}(R)$ can be calculated at the wall of the nozzle as:

$$\dot{\gamma}_{\max} = \left(\frac{dv}{dr}\right)_{r=R} = \frac{Q}{\pi R^3}\left(3+\frac{1}{n}\right) \tag{25}$$

By inserting the maximum shear rate in $\dot{\gamma}_{max}$ Equation (22), the maximum shear stress can be obtained:

$$\tau_{\max} = k_i\left(\frac{Q}{\pi R^3}\left(3+\frac{1}{n}\right)\right)^n \tag{26}$$

and the flow rate Q herein is calculated based on the nozzle dimeter of 0.686 mm (R) and printing speed of 1mm/s. This can be further represented as follows based on Equation (17) and the power-law index n as 0.2:

$$\tau_{\max} = \left[(k_{i\infty} - k_{i0})(1 - e^{-0.19 Y_{E/C} t}) + k_{i0} \right] \left(\frac{Q}{\pi R^3} \left(3 + \frac{1}{0.2} \right) \right)^{0.2} \tag{27}$$

Furthermore, the maximum shear stress can be estimated accordingly for the composite bioinks at the different cross-linking times as shown in **Figure 7c. Figure 7d** shows the cell viability as function of maximum shear stress based on the alamarBlue testing results. If the cell viability higher than 80% [60,61] is used to define the printability zone, the composite bioink must be printed by 1.65, 0.61, and 0.31 hours for the composite bioink with 1.00, 2.00, and 4.00% w/v TG, respectively, for these composite bioinks to have their maximum shear stress less than 1,275 Pa based on an exponentially fitted relationship ($1.17e^{-5.7\times10^{-4}\tau_{\max}}$) for 3T3 cells as seen from **Figure 7d**. Accordingly, the printability zone for satisfactory cell viability can be determined by meeting the following criterion:

$$e^{-0.19 Y_{E/C} t} \geq 0.78 \tag{28}$$

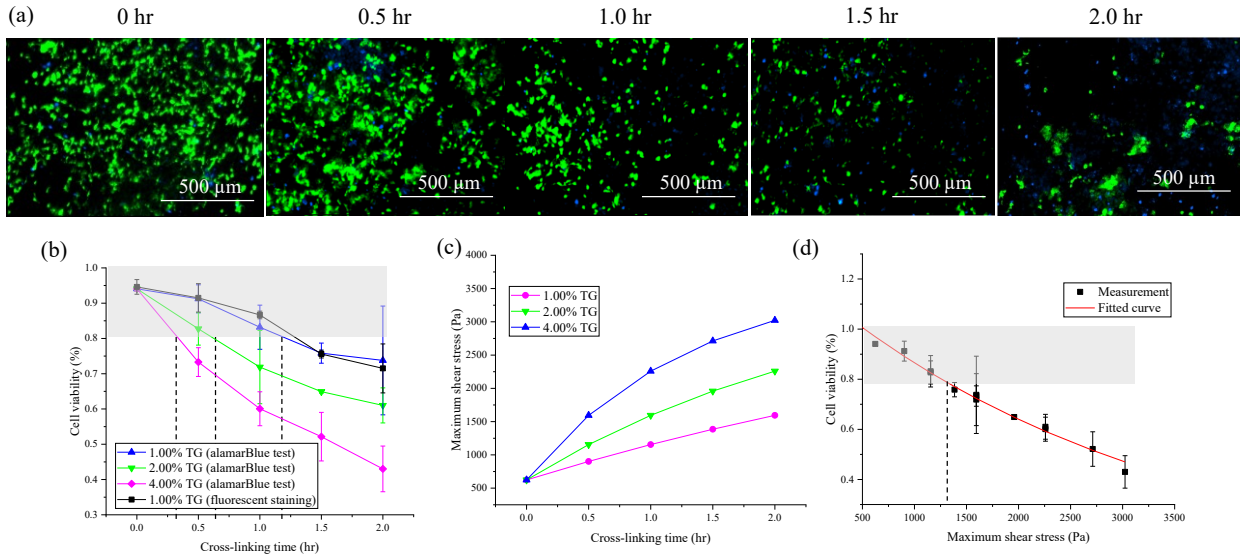

Figure 7. Cell viability evaluation. (a) Representative live/dead images of the cellular gelatin composite bioink with 1.00% w/v TG printed at different cross-linking times (green (live cells)

and blue (nuclei)) (scale bars: 500 μm). (b) Cell viability and (c) maximum shear stress as a function of cross-linking time. (d) The relationship between the cell viability and maximum shear stress.

5. Determination of TG-dependent Printability Zone

As proposed, the printability of the proposed gelatin microgel-gelatin solution composite bioink is evaluated based on the injectability, feature formability, and cell viability, which are all influenced by the TG concentration and its cross-linking time should be all considered as shown in **Figure 8a**. Based on the developed criteria (Equations (20), (21), and (28)), the printability zone per each criterion is shown in different colors (red, green, and yellow, respectively) in **Figure 8b**, and their overlapping region is the overall printability zone, which provides a guideline in selecting the printing time for a given TG concentration composite bioink. Within this overlapped printability zone, a successful and safe bioprinting process is expected.

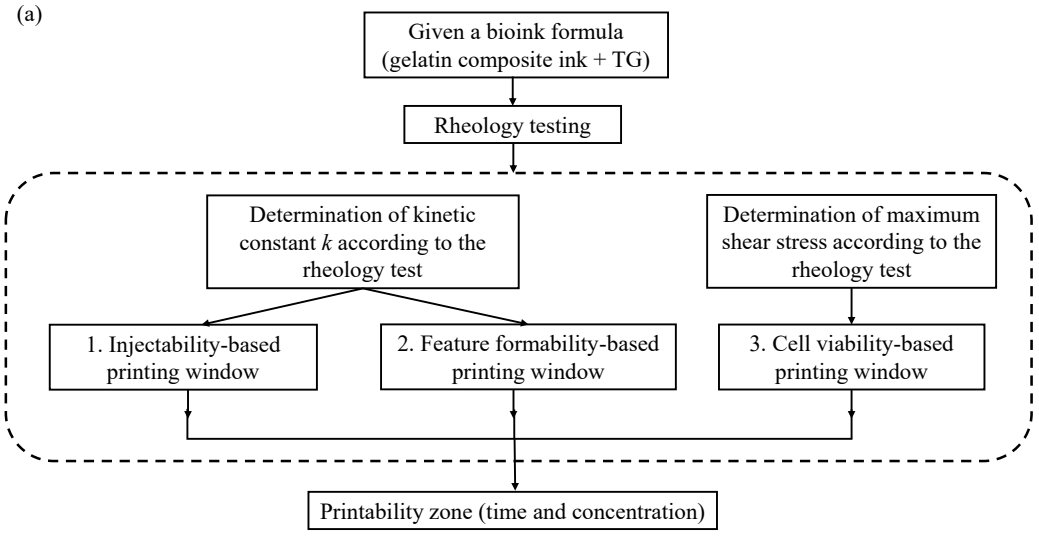

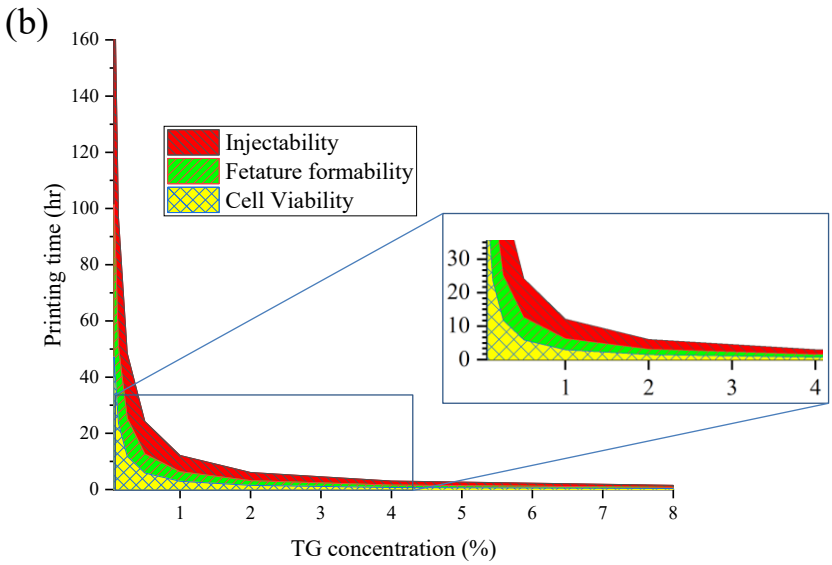

Figure 8. (a) Printability zone evaluation protocol and (b) the resultant printability zone based on the injectability (red area), feature formability (green area), and cell viability (yellow area).

6. Conclusions and Future Work

A composite bioink made of the discrete jammed gelatin microgel phase and the continuous TG cross-linkable gelatin precursor phase has been proved as a good bioink for bioprinting applications. Due to the inclusion of TG in the composite bioink, its rheological behavior varies over the time after the bioink is prepared, which is usually prepared right before a printing process. As such, the printing time is also the cross-linking time for the composite bioink. This work has systematically studied the printability of the gelatin microgel-gelatin solution composite bioink as functions of the TG concentration and cross-linking time, respectively, during extrusion bioprinting. To investigate the time-dependent rheological behavior of the gelatin composite bioink, the first-order kinetics of cross-linking processes has been utilized to model the rheology properties such as the storage modulus and viscosity as exponential functions of TG concentration

and cross-linking time. The bioink printability has been evaluated based on the following three metrics: injectability, feature formability, and process-induced cell injury, and each of them has been correlated to the determined rheological properties such as the storage modulus and/or viscosity as well as the rheological property-dependent shear stress. For a given corresponding threshold value, the good injectability zone, the good feature formability zone, and the satisfactory cell viability zone can be defined by exponential functions of TG concentration and cross-linking time, respectively. The overall printability zone can be identified by picking the overlapping zone of the injectability, feature formability, cell viability zones, providing a guideline for bioprinting process planning when the proposed gelatin microgel-gelatin solution composite bioink is used.

Future work may include the design and printing of gelatin composite constructs based on the identified printability zone and the identification of quantification approaches to determining the cross-linking degree of printed structures.

Acknowledgments

This study was partially supported by the US National Science Foundation (1762941), and the access of Anton Paar rheometers is acknowledged.

References:

[1] Murphy S V. and Atala A 2014 3D bioprinting of tissues and organs *Nat. Biotechnol.* **32** 773–85

[2] Huang Y, Leu M C, Mazumder J and Donmez A 2015 Additive manufacturing: Current state, future potential, gaps and needs, and recommendations *J. Manuf. Sci. Eng. Trans.*

ASME **137** 1–10

[3] Gu B K, Choi D J, Park S J, Kim M S, Kang C M and Kim C H 2016 3-Dimensional Bioprinting for Tissue Engineering Applications *Biomater. Res.* **20** 12

[4] Huang Y and Schmid S R 2018 Additive Manufacturing for Health: State of the Art, Gaps and Needs, and Recommendations *J. Manuf. Sci. Eng. Trans. ASME* **140** 9

[5] Zhang Z, Jin Y, Yin J, Xu C, Xiong R, Christensen K, Ringeisen B R, Chrisey D B and Huang Y 2018 Evaluation of bioink printability for bioprinting applications *Appl. Phys. Rev.* **5** 041304

[6] Jungst T, Smolan W, Schacht K, Scheibel T and Groll J 2016 Strategies and Molecular Design Criteria for 3D Printable Hydrogels *Chem. Rev.* **116** 1496–539

[7] Hölzl K, Lin S, Tytgat L, Van Vlierberghe S, Gu L and Ovsianikov A 2016 Bioink properties before, during and after 3D bioprinting *Biofabrication* **8** 032002

[8] Anthony A and Yoo J J 2015 Essentials of 3D biofabrication and translation *Academic Press*

[9] Klotz B J, Gawlitta D, Rosenberg A J W P, Malda J and Melchels F P W 2016 Gelatin-Methacryloyl Hydrogels: Towards Biofabrication-Based Tissue Repair *Trends Biotechnol.* **34** 394–407

[10] Kang H W, Tabata Y and Ikada Y 1999 Fabrication of porous gelatin scaffolds for tissue engineering *Biomaterials* **20** 1339–44

[11] Billiet T, Gevaert E, De Schryver T, Cornelissen M and Dubruel P 2014 The 3D printing of gelatin methacrylamide cell-laden tissue-engineered constructs with high cell viability *Biomaterials* **35** 49–62

[12] Echave M C, Burgo L S, Pedraz J L, and Orive G 2017 Gelatin as biomaterial for tissue engineering *Current pharmaceutical design* **24** 3567-84

[13] Irvine S A, Agrawal A, Lee B H, Chua H Y, Low K Y, Lau B C, Machluf M and Venkatraman S 2015 Printing cell-laden gelatin constructs by free-form fabrication and enzymatic protein crosslinking *Biomed. Microdevices* **17** 16

[14] Leber B, Mayrhauser U, Leopold B, Koestenbauer S, Tscheliessnigg K, Stadlbauer V, and Stiegler P 2012 Impact of temperature on cell death in a cell-culture model of hepatocellular carcinoma *Anticancer research* **32** 915-21

[15] Gedik C M, Ewen S W B, and Collins A R 1992 Single-cell gel electrophoresis applied to the analysis of UV-C damage and its repair in human cells *International journal of radiation biology* **62** 313-20

[16] Moné M J, Volker M, Nikaido O, Mullenders L H F, Van Zeeland A A, Verschure P J, Manders E M M and Van Driel R 2001 Local UV-induced DNA damage in cell nuclei results in local transcription inhibition *EMBO Rep.* **2** 1013–7

[17] Sinha R P and Häder D P 2002 UV-induced DNA damage and repair: A review *Photochem. Photobiol. Sci.* **1** 225–36

[18] Latonen L and Laiho M 2005 Cellular UV damage responses - Functions of tumor suppressor p53 *Biochim. Biophys. Acta - Rev. Cancer* **1755** 71–89

[19] Song K, Compaan A M, Chai W and Huang Y 2020 Injectable Gelatin Microgel-Based Composite Ink for 3D Bioprinting in Air *ACS Appl. Mater. Interfaces* **12** 22453–66

[20] Song K, Zhang D, Yin J and Huang Y 2021 Computational study of extrusion bioprinting with jammed gelatin microgel-based composite ink *Addit. Manuf.* **41** 101963

[21] Chen P Y, Yang K C, Wu C C, Yu J H, Lin F H and Sun J S 2014 Fabrication of large perfusable macroporous cell-laden hydrogel scaffolds using microbial transglutaminase *Acta Biomater.* **10** 912–20

[22] Zhu S, Stieger M A, van der Goot A J and Schutyser M A I 2019 Extrusion-based 3D printing of food pastes: Correlating rheological properties with printing behaviour *Innov. Food Sci. Emerg. Technol.* **58** 102214

[23] Paxton N, Smolan W, Böck T, Melchels F, Groll J and Jungst T 2017 Proposal to assess printability of bioinks for extrusion-based bioprinting and evaluation of rheological properties governing bioprintability *Biofabrication* **9** 044107

[24] Gao T, Gillispie G J, Copus J S, Kumar A P R, Seol Y J, Atala A, Yoo J J and Lee S J 2018 Optimization of gelatin-alginate composite bioink printability using rheological parameters: A systematic approach *Biofabrication* **10** 034106

[25] Liu Z, Bhandari B, Prakash S, Mantihal S and Zhang M 2019 Linking rheology and printability of a multicomponent gel system of carrageenan-xanthan-starch in extrusion based additive manufacturing *Food Hydrocoll.* **87** 413–24

[26] Diamantides N, Dugopolski C, Blahut E, Kennedy S and Bonassar L J 2019 High density cell seeding affects the rheology and printability of collagen bioinks *Biofabrication* **11** 045016

[27] Tan J J Y, Lee C P and Hashimoto M 2020 Preheating of gelatin improves its printability with transglutaminase in direct ink writing 3D printing *Int. J. Bioprinting* **6** 118–29

[28] Zhou M, Lee B H, Tan Y J and Tan L P 2019 Microbial transglutaminase induced controlled crosslinking of gelatin methacryloyl to tailor rheological properties for 3D printing *Biofabrication* **11** 025011

[29] Ledward D A 1986 Gelation of gelatin *Functional-Properties of Food Macromolecules* 171-201

[30] Clark A H and Ross-Murphy S B 2005 Structural and mechanical properties of biopolymer gels *Biopolymers* 57–192

[31] Chen T, Embree H D, Brown E M, Taylor M M and Payne G F 2003 Enzyme-catalyzed gel formation of gelatin and chitosan: Potential for in situ applications *Biomaterials* **24** 2831–41

[32] Choi Y S, Hong S R, Lee Y M, Song K W, Park M H and Nam Y S 1999 Study on gelatin-containing artificial skin: I. Preparation and characteristics of novel gelatin-alginate sponge *Biomaterials* **20** 409–17

[33] Ohtsuka T, Ota M, Nio N and Motoki M 2000 Comparison of substrate specificities of transglutaminases using synthetic peptides as acyl donors *Biosci. Biotechnol. Biochem.* **64** 2608–13

[34] Paguirigan A and Beebe D J 2006 Gelatin based microfluidic devices for cell culture *Lab Chip* **6** 407–13

[35] Srinivasan B 2020 Explicit Treatment of Non Michaelis-Menten and Atypical Kinetics in Early Drug Discovery *Preprints*

[36] Rogers A and Gibon Y 2009 Enzyme kinetics: theory and practice *Plant metabolic networks* 71-103

[37] Saguy I, Kopelman1 I J and Mizrahi S 1978 Thermal Kinetic Degradation of Betanin and Betalamic Acid *J. Agric. Food Chem.* **26** 360–2

[38] Kopelman R 1988 Fractal reaction kinetics *Science (80-.).* **241** 1620–6

[39] Fockink D H, Urio M B, Sánchez J H and Ramos L P 2017 Enzymatic Hydrolysis of Steam-

Treated Sugarcane Bagasse: Effect of Enzyme Loading and Substrate Total Solids on Its Fractal Kinetic Modeling and Rheological Properties *Energy and Fuels* **31** 6211–20

[40] Baek J, Fan Y, Jeong S H, Lee H Y, Jung H Do, Kim H E, Kim S and Jang T S 2018 Facile strategy involving low-temperature chemical cross-linking to enhance the physical and biological properties of hyaluronic acid hydrogel *Carbohydr. Polym.* **202** 545–53

[41] Bruno M, Giancone T, Torrieri E, Masi P and Moresi M 2008 Engineering properties of edible transglutaminase cross-linked caseinate-based films *Food Bioprocess Technol.* **1** 393–404

[42] O'Donnell J H and O'Sullivan P W 1981 A kinetic study of crosslinking vinyl polymerization by laser Raman spectroscopy - Free radical polymerization of diethylene glycol bis(allyl carbonate) *Polym. Bull.* **5** 103–10

[43] Nicoud L, Lattuada M, Lazzari S and Morbidelli M 2015 Viscosity scaling in concentrated dispersions and its impact on colloidal aggregation *Phys. Chem. Chem. Phys.* **17** 24392–402

[44] Farooqi Z H, Khalid R, Begum R, Farooq U, Wu Q S, Wu W T, Ajmal M, Irfan A, and Naseem K 2019 Facile synthesis of silver nanoparticles in a crosslinked polymeric system by in situ reduction method for catalytic reduction of 4-nitroaniline *Environmental technology* **40** 2027-36

[45] Rungseevijitprapa W and Bodmeier R 2009 Injectability of biodegradable in situ forming microparticle systems (ISM) *Eur. J. Pharm. Sci.* **36** 524–31

[46] Allmendinger A, Fischer S, Huwyler J, Mahler H C, Schwarb E, Zarraga I E and Mueller R 2014 Rheological characterization and injection forces of concentrated protein formulations: An alternative predictive model for non-Newtonian solutions *Eur. J. Pharm.*

Biopharm. **87** 318–28

[47] Krayukhina E, Fukuhara A and Uchiyama S 2020 Assessment of the Injection Performance of a Tapered Needle for Use in Prefilled Biopharmaceutical Products *J. Pharm. Sci.* **109** 515–23

[48] Suntornnond R, Tan E Y S, An J and Chua C K 2016 A Mathematical Model on the Resolution of Extrusion Bioprinting for the Development of New Bioinks *Materials (Basel).* **9** 756

[49] Koch F, Tröndle K, Finkenzeller G, Zengerle R, Zimmermann S and Koltay P 2020 Generic method of printing window adjustment for extrusion-based 3D-bioprinting to maintain high viability of mesenchymal stem cells in an alginate-gelatin hydrogel *Bioprinting* **20** e00094

[50] Darby R, Darby R, and Chhabra R P 2017 Chemical engineering fluid mechanics, revised and expanded *CRC Press*

[51] Liu Y, Zhang B, Xu Q, Hou Y, Seyedin S, Qin S, Wallace G G, Beirne S, Razal J M and Chen J 2018 Development of Graphene Oxide/Polyaniline Inks for High Performance Flexible Microsupercapacitors via Extrusion Printing *Adv. Funct. Mater.* **28** 1706592

[52] Gillispie G, Prim P, Copus J, Fisher J, Mikos A G, Yoo J J, Atala A and Lee S J 2020 Assessment methodologies for extrusion-based bioink printability *Biofabrication* **12** 022003

[53] Wang W, Huang Y, Grujicic M and Chrisey D B 2008 Study of impact-induced mechanical effects in cell Direct writing using smooth particle hydrodynamic method *J. Manuf. Sci. Eng. Trans. ASME* **130** 021012

[54] Wang W, Li G and Huang Y 2009 Modeling of bubble expansion-induced cell mechanical profile in laser-assisted cell direct writing *J. Manuf. Sci. Eng. Trans. ASME* **131** 051013

[55] Yin J and Huang Y 2011 Study of process-induced cell membrane stability in cell direct writing *J. Manuf. Sci. Eng. Trans. ASME* **133** 054501

[56] Zhang Z, Chai W, Xiong R, Zhou L and Huang Y 2017 Printing-induced cell injury evaluation during laser printing of 3T3 mouse fibroblasts *Biofabrication* **9** 025038

[57] Cidonio G, Glinka M, Dawson J I and Oreffo R O C 2019 The cell in the ink: Improving biofabrication by printing stem cells for skeletal regenerative medicine *Biomaterials* **209** 10–24

[58] Boularaoui S, Al Hussein G, Khan K A, Christoforou N and Stefanini C 2020 An overview of extrusion-based bioprinting with a focus on induced shear stress and its effect on cell viability *Bioprinting* **20** e00093

[59] Chhabra R P and Richardson J F 2011 Non-Newtonian flow and applied rheology: engineering applications *Butterworth-Heinemann*

[60] Rezvanian M, Tan C K, and Ng S F 2016 Simvastatin-loaded lyophilized wafers as a potential dressing for chronic wounds *Drug development and industrial pharmacy* **42** 2055-62

[61] Rajaratanam D D, Ariffin H, Hassan M A, Abd Rahman N M A N and Nishida H 2018 In vitro cytotoxicity of superheated steam hydrolyzed oligo((R)-3-hydroxybutyrate-co-(R)-3-hydroxyhexanoate) and characteristics of its blend with poly(L-lactic acid) for biomaterial applications *PLoS One* **13** e0199742